



HHS Public Access

Author manuscript

Br J Ophthalmol. Author manuscript; available in PMC 2019 February 01.

Published in final edited form as:

Br J Ophthalmol. 2018 February ; 102(2): 187–194. doi:10.1136/bjophthalmol-2016-309696.

Longitudinal characterisation of function and structure of Bietti crystalline dystrophy: report on a novel homozygous mutation in *CYP4V2*

Catherine M Lockhart¹, Travis B Smith², Paul Yang², Malini Naidu¹, Allan E Rettie³, Abhinav Nath³, Richard Weleber², and Edward J Kelly¹

¹Department of Pharmaceutics, University of Washington, Seattle, Washington, USA

²Casey Eye Institute, Oregon Health Sciences University, Portland, Oregon, USA

³Department of Medicinal Chemistry, University of Washington, Seattle, Washington, USA

Abstract

Background—Bietti crystalline dystrophy (BCD) is a rare inherited disorder characterised by fine crystalline deposits in the corneal limbus and retinal posterior pole. In 2004, mutations in the *CYP4V2* gene were identified as the cause of BCD. Here, we describe the report of a homozygous point mutation in a patient with BCD and provide detailed characterisation of functional and structural changes over 20 years.

Methods—At regular intervals, the patient underwent repeat ophthalmic evaluations. DNA was extracted from buccal swabs, amplified by standard PCR and analysed for homology to the *CYP4V2* sequence. Homology modelling was conducted using Iterative Threading ASSEMBly Refinement and molecular dynamics simulations using GRONingen MACHine for Chemical Simulations.

Results—The proband, a 47-year-old woman of German ancestry was diagnosed with crystalline retinopathy at age 25. Over the next 20 years, visual acuity and function gradually declined with progression of retinal pigment epithelium and choroidal atrophy. When first tested at 39 years of age, the multifocal electroretinogram (ERG) was markedly abnormal, more so for the right eye, whereas the full-field ERG was more symmetrical and lagged other measures of visual function.

Correspondence to Edward J Kelly, Department of Pharmaceutics, University of Washington, Seattle, WA 98195, USA; edkelly@uw.edu.

Contributors EJK, CML, TBS, PY, AER, AN and RW wrote and edited the manuscript. EJK, CML, TBS, PY, MN, AN and RW performed the work.

Competing interests Weleber is a consultant to Novartis, Pfizer and Wellstat; is a member of the scientific advisory board for Applied Genetic Technologies Corp; and serves on the scientific advisory board for the Foundation Fighting Blindness (the relationship has been reviewed and managed by Oregon Health and Science University). Dr Weleber also reports having received grants and personal fees from the Foundation Fighting Blindness and Applied Genetic Technologies Corp and other support from Sanofi, all outside the submitted work. In addition, Dr Weleber has a patent (US patent 8 657 446, method and apparatus for visual field monitoring, also known as Visual Field Monitoring and Analysis, or VFMA, which has not been issued).

Ethics approval OHSU and University of Washington Human Subjects Boards.

Provenance and peer review Not commissioned; externally peer reviewed.

Data sharing statement We will make available primary data used to generate the data in this manuscript in compliance with UW and OHSU Institutional regulations, including respective IRB committees. At this time, no further unpublished data on this patient is available for sharing.

Gene sequencing showed a single C>T point mutation in exon 9 encoding a R400C amino acid change. Computational modelling suggests the mutation impairs function due to loss of a hydrogen bonding interaction with the propionate side chains of the haeme prosthetic group.

Conclusion—This is the first report of a homozygous R400C mutation in *CYP4V2* with protein modelling showing high likelihood of enzyme dysfunction. The comprehensive long-term clinical follow-up provides insight into disease progression and highlights possible anti-inflammatory modulation of disease severity.

INTRODUCTION

Bietti crystalline dystrophy (BCD) is a rare inherited disorder characterised by fine crystalline deposits in the corneal limbus and retinal posterior pole.¹ Patients typically present with asymmetric symptoms of decreased visual acuity, impaired colour discrimination and nyctalopia in the second to third decade of life and subsequent visual field loss, abnormal electroretinogram (ERG) responses and legal blindness in the fifth to sixth decade of life. Progressive retinal degeneration involves the retinal pigment epithelium (RPE), choriocapillaris and photoreceptors and may be complicated by choroidal neovascularisation.

In 2004, researchers at the National Eye Institute identified mutations in the *CYP4V2* gene as the cause of BCD.² Cytochrome P450 4V2 (*CYP4V2*) is a member of a superfamily of haeme-containing mono-oxygenase enzymes.³ *CYP4V2* is ubiquitously expressed in humans, including liver and ocular tissues and has substrate selectivity for medium chain fatty acids; however, the enzyme's normal physiological function has yet to be elucidated.⁴ Since the genetic cause was first described, over 50 unique mutations have been identified throughout all 11 exons of *CYP4V2*.⁵ BCD is a genetically conferred disease, and transmission generally follows an autosomal recessive pattern, requiring two non-functional alleles.⁶ Here, we describe the report of a homozygous point mutation in exon 9 in a patient with BCD, and provide a detailed longitudinal characterisation of functional and structural changes.

MATERIALS AND METHODS

This study was conducted in accordance with the tenets of the Declaration of Helsinki and the study protocol was approved by the internal review board at Oregon Health and Science University (OHSU) and by the University of Washington Institutional Review Board. Written informed consent was obtained, and the patient was followed for 20 years at the Casey Eye Institute Oregon Retinal Degeneration Center at OHSU. At regular intervals, the patient underwent ophthalmic examination and testing, which included best-corrected visual acuity (BCVA), fundus colour photography, wide-field fundus autofluorescence (AF; Optos), wide-field fluorescein angiography (FA; Optos), semiautomated kinetic and automated static fullfield perimetry (Octopus 101/900, Haag-Streit), spectral-domain optical coherence tomography (OCT; Heidelberg Engineering), and ERG. Static perimetry was analysed and modelled as previously described.⁷ Full-field ERG (ffERG) recordings were obtained using Burian-Allen electrodes (Hansen Ophthalmic Development Laboratory) according to the International Society for Clinical Electrophysiology of Vision (ISCEV)

guidelines and as previously described.^{8,9} Multifocal ERG (mfERG) recordings were also obtained using Burian-Allen bipolar contact lens electrodes and performed according to the ISCEV guidelines¹⁰ using the Veris system (Electro-Diagnostic Imaging) with a protocol of 103 hexagons, 10–300 Hz bandpass filter and 8 min testing time divided into 60 s segments.

Statistics

Relationships and trends were explored using linear regression, the Screening Modelling Platform in JMP 12 (SAS Institute, Cary, North Carolina), linear and quadratic graphing and piecewise linear regression. Root mean square error (assessed variance and R^2 evaluated the goodness of fit. Extra-sum-of-squares F-tests determined the significance of slope values and slope differences between data sets. p Values below 0.05 were considered statistically significant.

PCR genotyping

DNA was extracted from buccal swabs from a patient with BCD and a healthy control with a Puregene DNA Isolation Kit following the manufacturer protocol (Gentra Systems, Minneapolis, Minnesota, USA). Each exon was individually amplified from extracted DNA by standard PCR with the following conditions listed in the online supplementary table.

Homology modelling

A homology model of wild-type CYP4V2 was constructed using the Iterative Threading ASSEmbly Refinement (I-TASSER) server,¹¹ which relies on both sequence and structural similarities to identify suitable templates for homology modelling from the Protein Data Bank. The highest ranked of five I-TASSER-derived models was selected for subsequent simulations. The R400C mutant was constructed in silico using the mutagenesis function in PyMol.

Molecular dynamics

All molecular dynamics (MD) simulations were performed in GRONingen MACHine for Chemical Simulations V.4.6.5.¹² Simulations employed the Gromos 54a7 force field parameter set with the simple point charge (SPC) explicit solvent model, and haeme-thiolate parameters adapted from published topologies.^{13,14} Initial homology models were energy minimised using iterative steepest descent and conjugate gradient methods until convergence was achieved. Short (2.5 ps) equilibration trajectories were performed on each starting model using a 0.5 fs time step, and then two independent production trajectories (50 ns each) were generated with a 2 fs time step using an NVT (constant temperature) ensemble. Structures were extracted every 50 ps for analysis.

RESULTS

Clinical structure and function

The proband is a 47-year-old woman of German ancestry and the only known affected member of her family. She first presented at age 25 with reduced visual acuity in the right eye of 20/50 (0.4 logMAR) and was diagnosed with crystalline retinopathy. Her history and

review of systems was not consistent with hyperoxaluria, cystinosis, drug toxicity, talc retinopathy or Sjogren-Larsson syndrome. She developed night vision difficulties at age 27 and reported more rapid vision loss during the course of two pregnancies. Over the next 20 years, the vision in the right eye continued to decline to a current BCVA of 20/200 (1.0 logMAR), whereas the vision in the left eye did not begin to decline until age 30 and is currently her better-seeing eye with BCVA of 20/50 (0.4 logMAR) (figure 1A). The progression of vision loss as measured by logMAR units was linearly correlated with age in each eye with goodness of fit ($R^2=0.9$). The regression line slopes were significant for both eyes (right: $p = 0.0017$, left: $p = 0.0012$) but were not significantly different from each other ($p = 0.15$). The pooled slope was $+0.024$ logMAR/year. Visual fields showed progressive loss of sensitivity, greater in the pericentral region between 10° and 20° from fixation, with eventual development of scotomas that deepened and enlarged with time (see online supplementary materials).

In contrast to the decline in visual acuity and visual fields, ffERGs were initially normal in both eyes at 27 years of age, slowly declined over time, became statistically significant at 39 years of age, following which time relatively symmetric progressive attenuation of rod-dependent and cone-dependent responses occurred in both eyes (figure 1 and online supplementary materials). At age 39, at a time when the ffERG was still roughly equal in both eyes, the mfERG showed markedly attenuated central macular cone-dependent function that was notably worse in the right eye (figure 1C). Consistent with BCVA and mfERG, kinetic perimetry also showed asymmetric central and paracentral scotomas with the III4e and V4e isopters that were worse in the right, which deepened and enlarged especially over the past several years (figure 2A). The III4e isopter area shows a progressively steep decline during ages 39–46 (figure 2B). Static perimetry (174-point grid, stimulus size V, German Adaptive Thresholding Estimation/GATE strategy) over the same time period showed similarly progressive decreases in sensitivity of both the central and peripheral fields (see online supplementary video 11). While retinal crystalline deposits were easily visualised on colour photography and infrared imaging (figure 3A,B), corneal limbal crystalline deposits did not manifest clinically until age 33. Wide-field AF revealed confluent hypoautofluorescence of the posterior pole, which correlated with extensive RPE atrophy in both eyes (figure 3C). At age 47, some intact macular autofluorescence remained, which correlates with residual RPE and better visual acuity in the left eye. Early phase wide-field FA show confluent hyperfluorescent window defect of the posterior pole with patchy hypofluorescent choroidal atrophy (figure 3D).

At age 44, she developed cystoid macular oedema (CME), which was worse in the right eye on OCT (figure 4A). Treatment with topical carbonic anhydrase inhibitor, 2% dorzolamide ophthalmic solution, reduced the CME over 6 months, but efficacy was limited by tachyphylaxis. At age 46, treatment with oral carbonic anhydrase inhibitor, acetazolamide 250 mg twice daily, for 6 months revealed near complete resolution of the CME in both eyes. However, during treatment her visual acuity was not significantly improved and eventually she could not tolerate the medication's systemic side effects. Shortly thereafter, she underwent sinus surgery with a 5-day course of oral corticosteroids and reported that her visual acuity improved dramatically, suggesting an inflammatory component to her vision loss. Late phase FA showed macular petalloid leakage mainly in the right eye (figure 4B).

Subsequent treatment of CME with topical corticosteroids, prednisolone acetate 1% thrice daily and topical non-steroidal anti-inflammatory, bromfenac 0.9% twice daily, showed partial effect in the right eye and no substantial effect in the left eye (figure 4A).

Gene sequencing

Sequencing *CYP4V2* in this BCD patient showed a single point mutation located in exon 9. The mutation is a C>T transversion (c.1198C>T), which results in an arginine to cysteine amino acid change at codon 400 in the protein. This R400C mutation was first reported by Lai *et al*, in 2007,¹⁵ but in that case the mutation was compound heterozygous with R400H. This is the first report of a homozygous point mutation at this location. The potential of the patient being hemizygous for *CYP4V2* was excluded using a quantitative PCR assay for gene copy number (data not shown).

Protein modelling

Molecular dynamics simulations indicate that our homology models of wild-type *CYP4V2* and the R400C mutant are globally stable conformations on the time scales accessible to computation. As shown in figure 5A, the root mean square deviation from the initial model, a measure of divergence from the starting state, rapidly (<10 ns) equilibrates for each of our MD trajectories and then remains at that plateau for the duration of the simulation. This behaviour is characteristic of well-behaved simulation systems and suggests the energy-minimised and equilibrated conformations of *CYP4V2* generated by our protocol are physically plausible models of the enzyme.

Computational modelling suggests an intriguing mechanism for the observed loss of function in the R400C mutant (see online supplementary video 22). In the wild-type homology model and MD trajectories, R400 is one of a handful of residues involved in hydrogen bonding interactions with the propionate side chains of the haeme prosthetic group. The R400C mutant is no longer capable of hydrogen bonding to the propionate groups, as indicated by the increased distance to the haeme plotted in figure 5B. One might expect the loss of this stabilising interaction to perturb the local environment around the haeme. Indeed, in one of our R400C simulations, we observed a dramatic and rapid rearrangement of the haeme: from its initial orientation facing the active site, the haeme flips outward by ~70° so as to expose the propionate group to solvent (figure 5C,D). The loss of favourable R400-haeme interactions thus appears to trigger a compensatory rearrangement of *CYP4V2* that leaves it in a presumably inactive, or at least highly perturbed, state, with the haeme iron partially occluded and facing away from the active site. Importantly, rearrangements of the protein backbone are limited to residues relatively close to the haeme, with the overall fold of *CYP4V2* being maintained in our simulation.

Of course, the biological situation is likely considerably more complex than the mechanism outlined in our MD trajectories for several reasons. First, our initial structures are homology models that, while physically plausible and stable in silico, are necessarily more tentative guesses at the structure of *CYP4V2* than an experimentally determined crystal structure would be. Second, our model does not account for the effect of the biological environment, particularly incorporation into a membrane, on the structure of *CYP4V2*. Third, some

CYP4B isoforms are known to display a significant degree of covalent haeme adduction to a glutamate residue on the I-helix that would presumably decrease the likelihood of haeme rearrangement on the loss of hydrogen bonding to R400.¹⁶ It is unclear to what extent CYP4V2 displays this modification, although the homologous glutamate (E329) is well placed to conjugate the haeme in our homology model. If wild-type CYP4V2 does display a significant degree of covalent haeme adduction, then the R400C mutant might exert its activity in two ways: by inhibiting the initial folding of the enzyme into a conformation capable of haeme adduction, or by inactivating the fraction of CYP4V2 that fails to conjugate the haeme even after proper folding. In either case, our computational modelling provides clear support for the idea that R400 is a key residue in stabilising the haeme and positioning it for catalysis, and that the R400C mutant would be disrupted in its structure and function by the loss of a hydrogen bond donor in this position. Supporting this conclusion is the fact that sequence homology-based algorithms also predict the R400C mutation to be highly disruptive (PROVEAN V.1.1.3 (<https://doi.org/10.1093/bioinformatics/btv195>) score = -7.66, SIFT (<https://www.ncbi.nlm.nih.gov/pubmed/19561590>.) score = 0.00.

DISCUSSION

The case described here is one of the most extensive longitudinal characterisations of structure and function in BCD, especially with regard to the correlation of visual acuity, visual fields and ffERG. To date, there have been only a few published cases of long-term studies in BCD.¹⁷⁻²⁰ Of those, only two also report a clinical follow-up longer than 20 years, namely Mansour and colleagues (25 years) and Bagolini and Ioli-Spada (30 years). Our case is consistent with prior reports in that visual acuity declines with progression of RPE and choroidal atrophy and development of scotomas on both kinetic and static testing. Our patient had distinctive pericentral loss of visual field sensitivity on static testing (see online supplementary materials). We found the mfERG to be markedly abnormal at the first time it was performed. In agreement with other reports,^{21, 22} the ffERG amplitudes are not as severely abnormal at the time of initial testing, can lag other measures of retinal function and the attenuation with time is less than is often occurs with other more common forms of inherited retinal degenerations, such as retinitis pigmentosa. Also, although not previously emphasised, unlike typical forms of retinitis pigmentosa, the b-wave implicit times of the rod and cone components of the ffERG were not markedly delayed in our patient as is very often the case in typical forms of retinitis pigmentosa and other inherited choroidal atrophies.

In addition, we show that the rate of decline in visual acuity was surprisingly similar for both eyes irrespective of baseline acuity, suggesting that the rate of macular degeneration is the same even if one eye lags the other. We also used wide-field AF and wide-field FA to show that RPE and choroidal atrophy in BCD was extensive and concentrated in the posterior pole up to the fifth decade of life. Moreover, we report for the first time, to our knowledge, the longterm dynamics of full-field kinetic and static perimetry in BCD, which showed expanding and deepening pericentral and central scotomas. Long-term follow-up of the III4e isopter area revealed that the rate of constriction appeared to increase after age 44, which, incidentally, is the age the patient, developed CME. Indeed, it is unknown if

treatment of CME had any effect on the rate of progression of either visual acuity or visual fields. As reported in other BCD cases,²³ carbonic anhydrase inhibitors were effective in reducing CME, but can be limited by tachyphylaxis and systemic side effects. We also report for the first time that topical anti-inflammatory medications may have a partial effect on CME that is associated with significant leakage on FA but has no effect on non-leaking CME. A screening modelling analysis using JMP 12 (see online supplementary materials) detected an overall greater loss for LogMAR BCVA for the right eye, and detected a signal of significant worsening around the time of the the event, as defined by the date of surgery. Comparative linear and quadratic graphic fitting of V_{tot} , and to a much lesser degree, V_{30° , suggested the presence of the event around the time of the surgery. Piecewise linear regression more precisely defined the effect of the Event on V_{tot} and determined its significance (see online supplementary materials).

The prevalence of non-neovascular BCD-associated CME is low and its pathogenesis is poorly understood²⁴; however, our experience in this case suggests a possible component of inflammation influencing the course of the disease progression. Additional studies are needed to further elucidate the role of anti-inflammatory therapy in BCD with CME.

There are limitations to the in silico protein model. This simulation is from a homology model, and there is not yet independent experimental evidence that the starting configuration is accurate. Even starting from an accurate model, MD simulations are themselves not 100% accurate at predicting protein dynamics. Even if they were, 50 ns is a very short time scale compared with the seconds and minutes that are relevant to catalysis, and longer simulations could show more diverse behaviour. Finally, other CYP4s can (some fraction of the time) form a covalent linkage from the I-helix to the haeme that could affect this behaviour; the effect of this covalent linkage will be modelled in future work. Despite these caveats, it is still plausible that a mutation such as R400C could disrupt the hydrogen bond network around the haeme and significantly perturb 4V2 conformation and hence function, either during initial folding/haeme incorporation or for the mature protein.

In conclusion, we present a rare report of a detailed long-term follow-up of BCD, utilising visual function tests and multimodal imaging to provide insight into the dynamics of disease progression in BCD. This case of BCD is complicated by CME, which is responsive to carbonic anhydrase inhibitors and partially responsive to topical anti-inflammatory medications, suggesting a potential inflammatory component to the oedema. Moreover, this is the first report of a homozygous R400C mutation in CYP4V2 with protein modelling showing a high likelihood of enzyme dysfunction.

Supplementary Material

Refer to Web version on PubMed Central for supplementary material.

Acknowledgments

Funding This work was supported by grants CD-NMT-0714-0648-OHSU (Dr Yang) from the Foundation Fighting Blindness, grant 1K08EY026650-01 from the National Institutes of Health (Dr Yang), core grant P30EY010572 and unrestricted grant C-CL-071 1-0534-OHSU01 from the Foundation Fighting Blindness (Casey Eye Institute) and an unrestricted grant from Research to Prevent Blindness (Casey Eye Institute). This publication was supported

by the National Center For Advancing Translational Sciences of the National Institutes of Health under Award Number UL1TR000423 (Drs Lockhart and Kelly).

REFERENCES

1. Ng DS, Lai TY, Ng TK, et al. Genetics of Bietti crystalline dystrophy. *Asia Pac J Ophthalmol* 2016;5:245–52.
2. Li A, Jiao X, Munier FL, et al. Bietti crystalline corneoretinal dystrophy is caused by mutations in the novel gene CYP4V2. *Am J Hum Genet* 2004;74:817–26. [PubMed: 15042513]
3. Kelly EJ, Nakano M, Rohatgi P, et al. Finding homes for orphan cytochrome P450s: cyp4v2 and CYP4F22 in disease states. *Mol Interv* 2011;11:124–32. [PubMed: 21540472]
4. Nakano M, Kelly EJ, Wiek C, et al. CYP4V2 in Bietti's crystalline dystrophy: ocular localization, metabolism of omega-3-polyunsaturated fatty acids, and functional deficit of the p.H331P variant. *Mol Pharmacol* 2012;82:679–86. [PubMed: 22772592]
5. Lockhart CM, Nakano M, Rettie AE, et al. Generation and characterization of a murine model of Bietti crystalline dystrophy. *Invest Ophthalmol Vis Sci* 2014;55:5572–81. [PubMed: 25118264]
6. Kaiser-Kupfer MI, Chan CC, Markello TC, et al. Clinical biochemical and pathologic correlations in Bietti's crystalline dystrophy. *Am J Ophthalmol* 1994;118:569–82. [PubMed: 7977570]
7. Weleber RG, Smith TB, Peters D, et al. VFMA: topographic analysis of sensitivity data from full-field static perimetry. *Transl Vis Sci Technol* 2015;4:14.
8. Marmor MF, Fulton AB, Holder GE, et al. ISCEV Standard for full-field clinical electroretinography (2008 update). *Doc Ophthalmol* 2009;118:69–77. [PubMed: 19030905]
9. Oh KT, Weleber RG, Stone EM, et al. Electroretinographic findings in patients with stargardt disease and fundus flavimaculatus. *Retina* 2004;24:920–8. [PubMed: 15579991]
10. Hood DC, Bach M, Brigell M, et al. ISCEV standard for clinical multifocal electroretinography (mfERG) (2011 edition). *Doc Ophthalmol* 2012;124:1–13.
11. Zhang Y I-TASSER server for protein 3D structure prediction. *BMC Bioinformatics* 2008;9:40. [PubMed: 18215316]
12. Pronk S, Páll S, Schulz R, et al. GROMACS 4.5: a high-throughput and highly parallel open source molecular simulation toolkit. *Bioinformatics* 2013;29:845–54. [PubMed: 23407358]
13. Oda A, Yamaotsu N, Hirono S. New AMBER force field parameters of heme iron for cytochrome P450s determined by quantum chemical calculations of simplified models. *J Comput Chem* 2005;26:818–26. [PubMed: 15812779]
14. Roberts AG, Cheesman MJ, Primak A, et al. Intramolecular heme ligation of the cytochrome P450 2c9 R108H mutant demonstrates pronounced conformational flexibility of the B-C loop region: implications for substrate binding. *Biochemistry* 2010;49:8700–8. [PubMed: 20815369]
15. Lai TY, Ng TK, Tam PO, et al. Genotype phenotype analysis of Bietti's crystalline dystrophy in patients with CYP4V2 mutations. *Invest Ophthalmol Vis Sci* 2007;48:5212–20. [PubMed: 17962476]
16. Baer BR, Schuman JT, Campbell AP, et al. Sites of covalent attachment of CYP4 enzymes to heme: evidence for microheterogeneity of P450 heme orientation. *Biochemistry* 2005;44:13914–20. [PubMed: 16229480]
17. Bernauer W, Daicker B. Bietti's corneal-retinal dystrophy. A 16-year progression. *Retina* 1992;12:18–20. [PubMed: 1565865]
18. Jurklies B, Jurklies C, Schmidt U, et al. (Corneoretinal dystrophy (Bietti)-Long-term course of one patient over a period of 30 years, and interindividual variability of clinical and electrophysiological findings in two patients). *Klin Monbl Augenheilkd* 2001;218:562–9. [PubMed: 11573158]
19. Mansour AM, Uwaydat SH, Chan CC. Long-term follow-up in Bietti crystalline dystrophy. *Eur J Ophthalmol* 2007;17:680–2. [PubMed: 17671952]
20. Sánchez Vicente JL, Herrador Montiel A, Díez-Garretas C, et al. (Bietti's crystalline dystrophy. A 5-year progression). *Arch Soc Esp Oftalmol* 2001;76:323–6. [PubMed: 11373710]
21. Halford S, Liew G, Mackay DS, et al. Detailed phenotypic and genotypic characterization of bietti crystalline dystrophy. *Ophthalmology* 2014;121:1174–84. [PubMed: 24480711]

22. Rossi S, Testa F, Li A, et al. Clinical and genetic features in Italian Bietti crystalline dystrophy patients. *Br J Ophthalmol* 2013;97:174–9. [PubMed: 23221965]
23. Broadhead GK, Chang AA. Acetazolamide for cystoid macular oedema in Bietti crystalline retinal dystrophy. *Korean J Ophthalmol* 2014;28:189–91. [PubMed: 24688265]
24. Li Q, Li Y, Zhang X, et al. Utilization of fundus autofluorescence, spectral domain optical coherence tomography, and enhanced depth imaging in the characterization of Bietti crystalline dystrophy in different stages. *Retina* 2015;35:2074–84. [PubMed: 25978730]

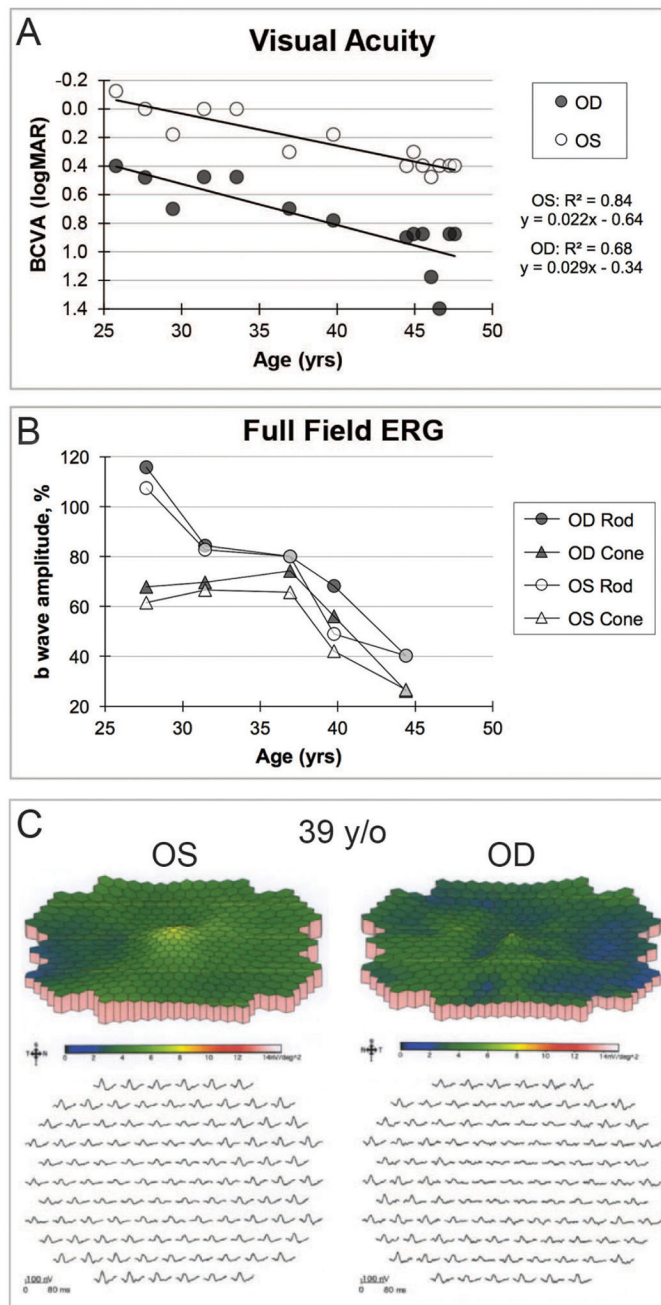


Figure 1. (A) BCVA over time with best-fit line depicting progressive decline with slope in each eye that was significantly different than zero but not significantly different than each other. The last two BCVA measurements were made within months following the surgery. Improvement from 20/500 to 20/50 occurred for the right eye, whereas the BCVA for the left eye was essentially unchanged from the previous measurements prior to the surgery. (B) Rod b-wave amplitude response to dim white light and cone b-wave amplitude response to photopic bright flash stimuli. Both rod and cone photoreceptor-dependent full-field ERG responses declined and were significantly below normal at 39 years of age in each eye.

Progression for each photoreceptor-mediated amplitude is presented as the percentage of the patient's amplitude compared with the normal mean value. (C) Multifocal ERG, performed at 39 years of age, showed diffuse attenuation of amplitude densities that was greater for the right eye. BCVA, best-corrected visual acuity; ERG, electroretinogram; OD, right eye; OS, left eye; y/o, years old; yrs, years.

Author Manuscript

Author Manuscript

Author Manuscript

Author Manuscript

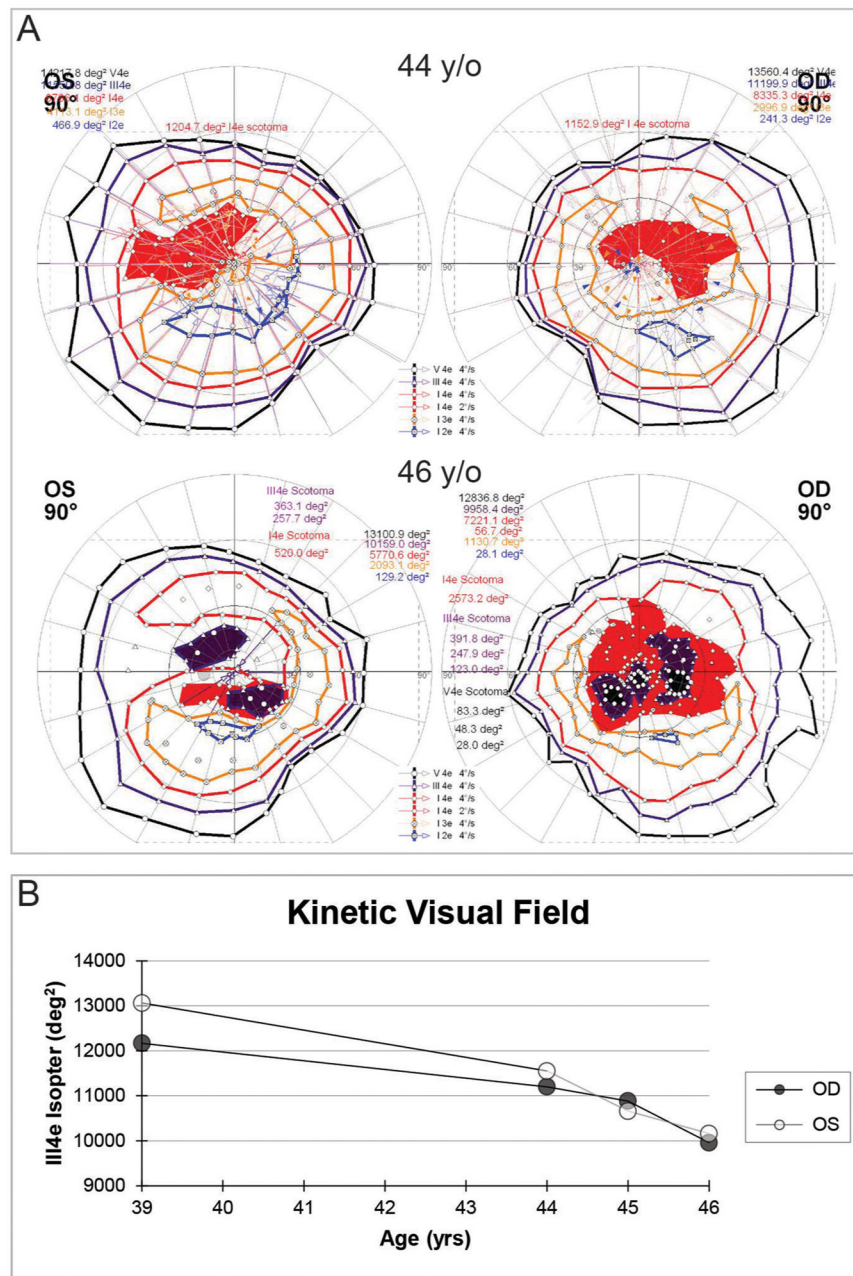


Figure 2. (A) Kinetic perimetry shows rapid development of worsening central and pericentral scotomas over the course of 2 years. (B) The area of the III4e isopter plotted over time showed a progressive decline in both eyes. deg², squared degrees; OD, right eye; OS, left eye; y/o, years old; yrs, years.

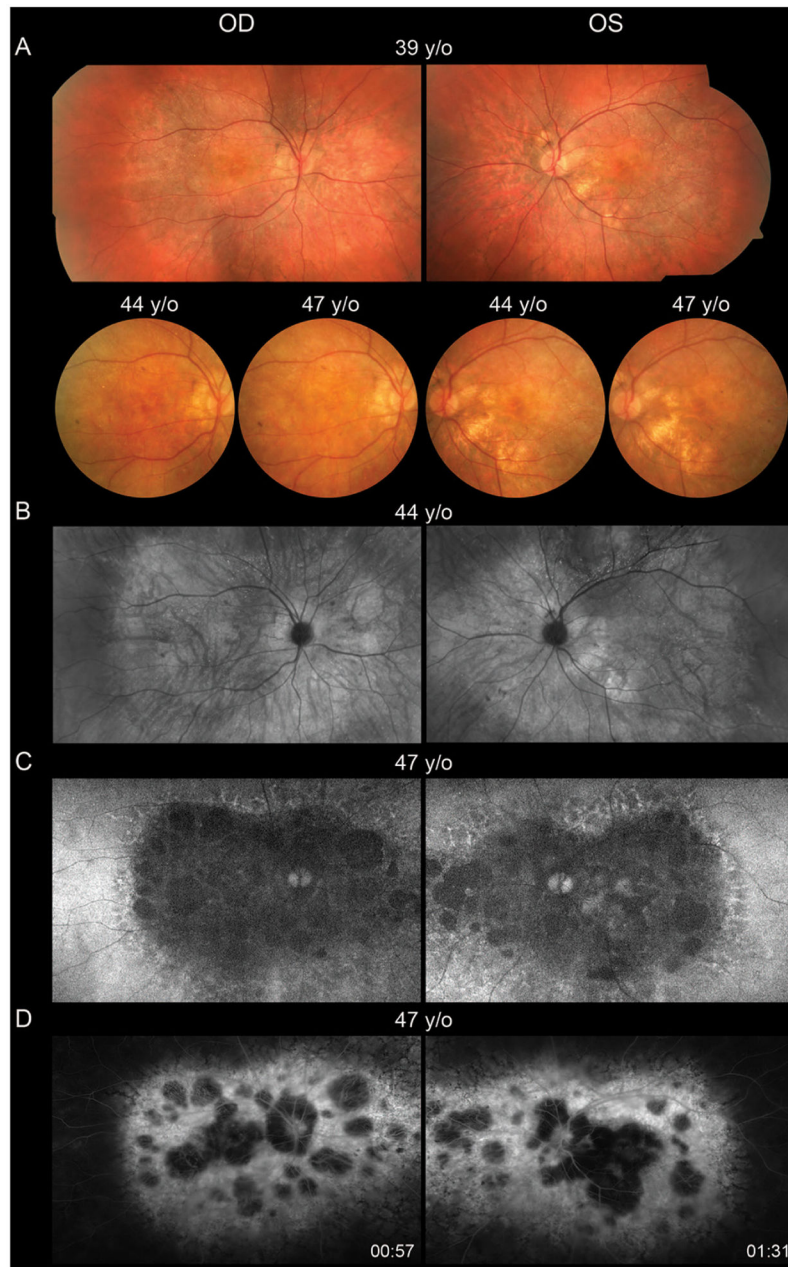


Figure 3.

(A) Colour fundus photography show posterior pole crystalline deposits and confluent retinal atrophy, which progresses over time. (B) Montage of infrared images highlights the crystalline deposits and areas of retinal atrophy. (C) Wide-field autofluorescence shows confluent heterogeneous hypoautofluorescence throughout the posterior pole, which is surrounded by lacey hyperfluorescence throughout the midperipheral transition zone. (D) Early-phase wide-field fluorescein angiography shows confluent hyperfluorescent window defect of the posterior pole with patchy hypofluorescent choroidal atrophy. OD, right eye; OS, left eye; y/o, years old.

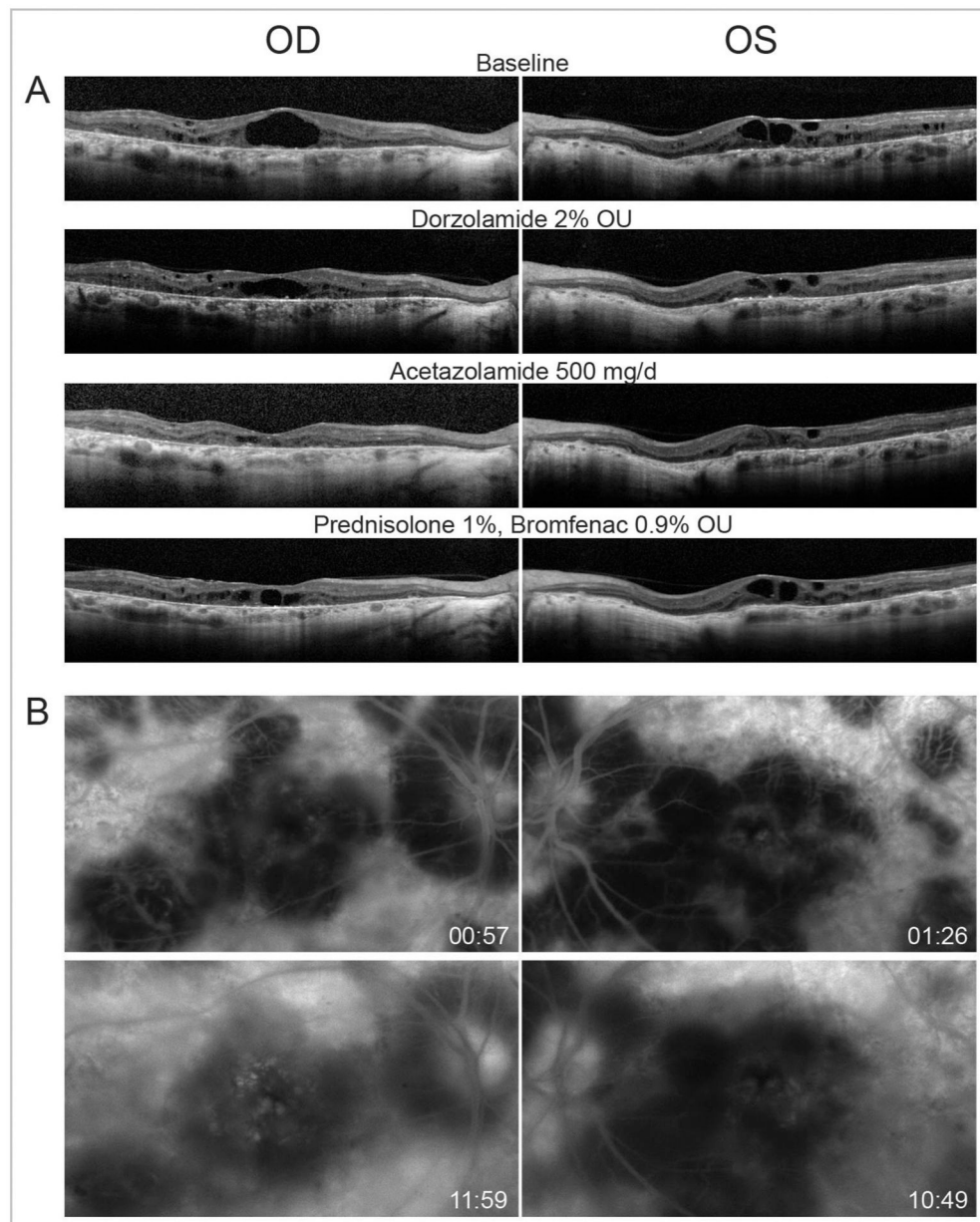


Figure 4.

(A) Optical coherence tomography. Horizontal linear B scans through the fovea show cystoid macular oedema in both eyes at baseline and response to treatment. Retinal pigment epithelial atrophy and outer retinal attenuation with outer retinal tubulations are also observed. (B) Fluorescein angiography show late leakage mainly in the right eye. Hyperfluorescent window defect and hypofluorescent choroidal atrophy are also evident. OD, right eye; OS, left eye; OU, both eyes; mg/d, milligrams per day.

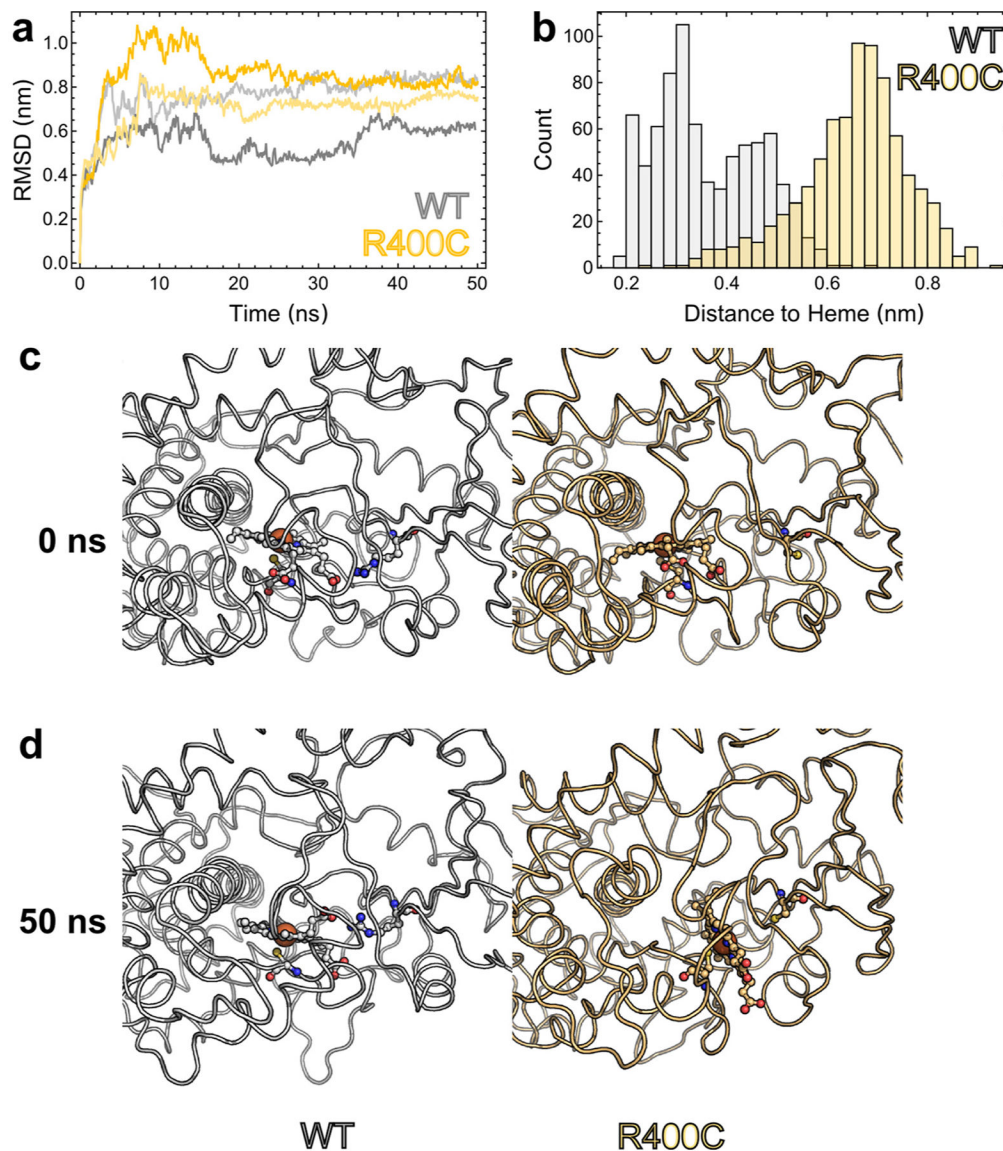


Figure 5. Computational comparison of wild-type CYP4V2 with the R400C mutant. (A) RMSD of each trajectory from its starting structure serves to demonstrate that our homology models can feasibly be studied by computational means. The RMSD rapidly achieves a plateau, indicating that the protein as a whole has assumed a locally stable conformation in silico. (B) Histogram of shortest distances between residue 400 and the haeme for each frame of our wild-type and mutant simulations. The wild-type R400 interacts much more closely with the haeme group and spends the majority of its time within hydrogen-bonding distance of the haeme propionates. In contrast, the R400C mutant has lost these interactions and is much more distant from the haeme. (C) Initial states of our simulated system, with wild-type (white) on the left and R400C (pale orange) on the right. Both enzymes are in highly similar conformations, with the haeme facing the active site and apparently available for catalysis. The peptide backbone is shown as a loop, while residue 400, the haeme prosthetic group and the thiolate ligand (C467) are depicted with ball-and-stick representation. (D) An illustration

of the dramatic changes that can result from the loss of R400. After 50 ns of simulation, the haeme orientation is essentially unchanged in wtCYP4V2, but has everted by $\sim 70^\circ$ in the R400C mutant, presumably contributing to diminished stability or catalytic activity. RMSD, root mean square deviation.

Author Manuscript

Author Manuscript

Author Manuscript

Author Manuscript